

Strongly Interacting Matter at Very High Energy Density: 3 Lectures in Zakopane*

LARRY McLERRAN

Brookhaven National Laboratory and Riken Brookhaven Center
Physics Dept. PO Box 5000
Upton, NY, 99673, USA

AND

These lectures concern the properties of strongly interacting matter at very high energy density. I begin with the Color Glass Condensate and the Glasma, matter that controls the earliest times in hadronic collisions. I then describe the Quark Gluon Plasma, matter produced from the thermalized remnants of the Glasma. Finally, I describe high density baryonic matter, in particular Quarkyonic matter. The discussion will be intuitive and based on simple structural aspects of QCD. There will be some discussion of experimental tests of these ideas.

1. Introduction

These lectures concern the properties of strongly interacting matter at high energy density. Such matter occurs in a number of contexts. The high density partonic matter that controls the early stages of hadronic collisions at very high energies is largely made of very coherent gluonic fields. In a single hadron, such matter forms the small x part of a wavefunction, a Color Glass Condensate. After a collision of two hadrons, this matter almost instantaneously is transformed into longitudinal color electric and color magnetic fields. The ensemble of these fields in their early time evolution is called the Glasma. The decay products of these fields thermalize and form a high temperature gas of quarks and gluons, the Quark Gluon Plasma. In collisions at lower energy, and perhaps in naturally occurring objects such as neutron stars, there is high baryon density matter at low temperature. This is Quarkyonic matter.

* Presented at the 50'th Crakow School of Theoretical Physics, Zakopane, Poland, June 2010

There is a very well developed literature concerning these various forms of matter. It is not the purpose of these lectures to provide a comprehensive review. I will concentrate on motivating and describing such matter from simple intuitive physical pictures and from simple structural aspects of QCD. I will attempt at various places to relate what is conjectured or understood about such matter to experimental results from accelerator experiments.

2. Lecture I: The Color Glass Condensate and the Glasma

The parton distributions of gluons, valence quarks and sea quarks can be measured for some momentum scale less than a resolution scale Q as a function of their fractional momentum x of a high energy hadron. The lowest value of x accessible for a fixed hadron energy E is typically $x_{min} \sim \Lambda_{QCD}/E_{hadron}$. The small x limit is therefore the high energy limit.

It is remarkable that as x is decreased, as we go to the high energy limit, that the gluon density dominates the constituents of a hadron for $x \leq 10^{-1}$. The various distributions are shown as a function of x in Fig. 1. The gluon density rises like a power of x like $x^{-\delta}$, $\delta \sim .2 - .3$ at accessible energies. The

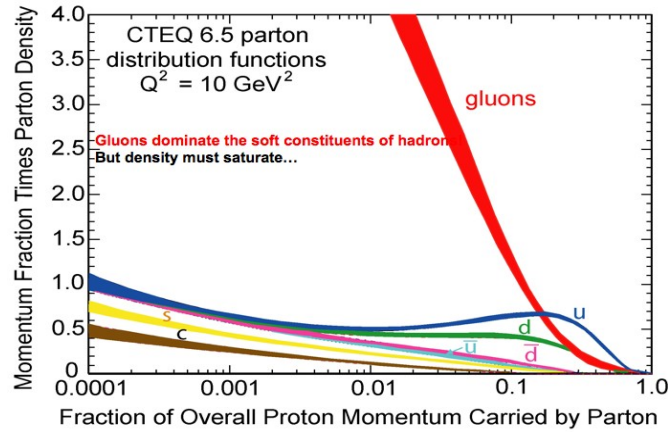


Fig. 1. The parton distribution as a function of x .

area of a hadron grows slowly with energies. Cross sections grow roughly as $\ln^2(1/x)$ for small x . This means that the rapidly growing gluon distribution results in a high density system of gluons. At high density, the gluons have small separation and by asymptotic freedom, the intrinsic strength of their interaction must be weak.

A small intrinsic interaction strength does not mean that interactions

are weak. Consider gravity: The interactions between single protons is very weak, but the force of gravity is long range, and the protons in the earth act coherently, that is always with the same sign. This results in a large force of gravity. This can also happen for the gluons inside a hadron, if their interactions are coherent.

To understand how this might happen, suppose we consider gluons of a fixed size $r_0 \sim 1/p_T$ where p_T is its transverse momentum. We assume that at high energy, the gluons have been Lorentz contracted into a thin sheet, so we need only consider the distribution of gluons in the transverse plane. If we start with a low density of gluons at some energy, and then evolve to higher energy, the density of gluons increases. When the density is of order one gluon per size of the gluon, the interaction remains weak because of asymptotic freedom. When the density is of order $1/\alpha_S$, the coherent interactions are strong, and adding another gluon to the system is resisted by a force of order 1. The gluons act as hard spheres. One can add no more gluons to the system of this size. It is however possible to add in smaller gluons, in the space between the closely packed gluons of size r_0 . This is shown in Fig. 2

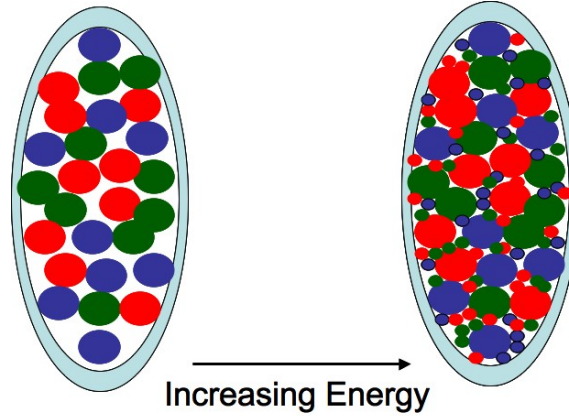


Fig. 2. Increasing the gluon density in a saturated hadron when going to higher energy.

The physical picture we derive means that below a certain momentum scale, the saturation scale Q_{sat} , the gluon density is saturated and above this scale it is diffuse. The saturation momentum scale grows with energy and need not itself saturate[1]-[4].

The high phase space density of gluons, $dN/dy d^2 p_T d^2 r_T \sim 1/\alpha_S$ suggests that one can describe the gluons as a classical field. A phase space

density has a quantum mechanical interpretation as density of occupation of quantum mechanical states. When the occupation number is large, one is in the classical limit.

One can imagine this high density gluon field generated from higher momentum partons. We introduce the idea of sources corresponding to high x partons and fields as low x partons. Because the high x parton sources are fast moving, their evolution in time is Lorentz time dilated. The gluon field produced by these sources is therefore static and evolves slowly compared to its natural time scale of evolution. This ultimately means that the different configurations of sources are summed over incoherently, as in a spin glass.

We call this high energy density configuration of colored fields a Color Glass Condensate. The word color is because the gluons that make it are colored. The word condensate is used because the phase space density of gluons is large, and because this density is generated spontaneously. The word glass is used because the typical time scale of evolution of the classical fields is short compared to the Lorentz time dilated scales associated with the sources of color.

There is an elaborate literature on the Color Glass Condensate and an excellent review is by Iancu and Venugopalan[5]. Evolution of the CGC to small values of x is understood, as well as many relationships between deep inelastic scattering, deep inelastic diffraction and high energy nucleus-nucleus, proton-nucleus and proton-proton scattering. The CGC is a universal form of matter in the high energy limit. The theoretical ideas underlying the CGC are largely unchallenged as a description of the high energy limit of QCD, but the issue of when the approximation appropriate for the high energy limit are valid remains contentious.

In the description of high energy hadron hadron collisions, we consider the collision of two sheets of CGC as shown in Fig. 3. The color electric and color magnetic fields of the CGC are visualized as sheets of Lenard-Wiechart potentials. These are classical gluon fields whose polarization and color are random, with an intensity distribution determined by the underlying theory of the CGC.

Upon collision of these sheets, the sheets become charged with color magnetic and color electric charge distributions of equal magnitude but opposite sign locally in the transverse plane of the sheets[6]-[13]. In the high energy limit sources of color electric and color magnetic field must be treated on an equal footing because of the self duality of QCD. This induced charge density produces longitudinal color electric and color magnetic fields between the two sheets. These fields are longitudinally boost invariant and therefore have the correct structure to account for Bjorken's initial conditions in heavy ion collisions[14]. The typical transverse length scale over which the flux tubes vary is $1/Q_{sat}$. The initial density of produced gluons

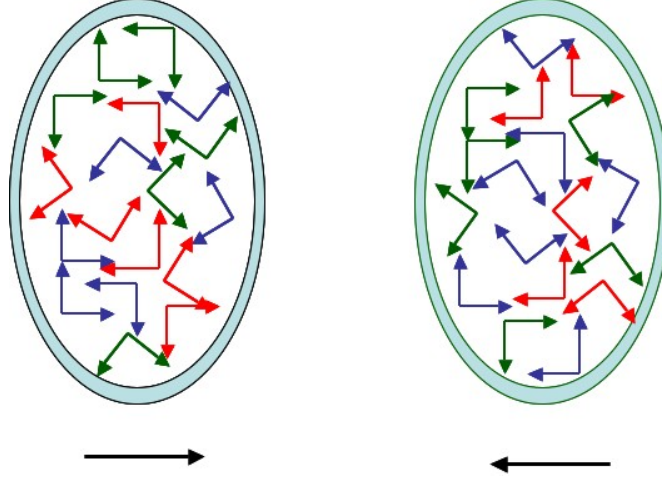


Fig. 3. The collision of two sheets of CGC.

is on dimensional grounds

$$\frac{1}{\pi R^2} \frac{dN}{dy} \sim \frac{Q_{sat}^2}{\alpha_S} \quad (1)$$

Because there are both color electric and color magnetic fields, there is a topological charge density of maximal strength induced $FF^D \sim Q_{sat}^2/\alpha_S$

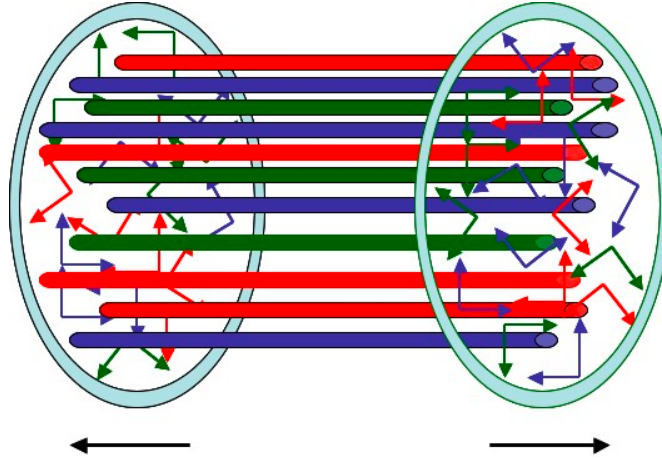


Fig. 4. Glasma flux tube produces after the collision.

The decay of products of the Glasma is what presumably makes a thermalized Quark Gluon Plasma. It is not clear how this thermalization takes place. It is quite likely that in the decay of these fields, a turbulent fluid arises, and perhaps this fluid can generate an expansion dynamics similar to that of a thermalized QGP for at least some time[15].

2.1. The CGC and Electron-Hadron Scattering

If the only momentum scale that controls high energy scattering is the saturation momentum, then there will be scaling[16]. In particular, the cross section for deep inelastic scattering will be a function

$$\sigma_{\gamma^*p} \sim F(Q^2/Q_{sat}^2) \quad (2)$$

rather than a function of Q^2 and x independently. The x dependence of the saturation momentum may be determined empirically as $Q_{sat}^2 \sim Q_0^2/x^\delta$ where $\delta = 0.2 - 0.3$, which is consistent with analysis of evolution equations[17]-[26]. The scaling relationship can be derived from the classical theory for $Q^2 \leq Q_{sat}^2$. It can further be shown to extend over a much larger range of Q^2 [27]. For large values of Q^2 this scaling is a consequence of the linear evolution equations, but the global structure is determined by the physics of saturation. Such a simple scaling relationship describes deep inelastic scattering data for $x \leq 10^{-2}$.

Using evolution equations for the CGC including the effects of running coupling constant[28]-[29], one can compute deep inelastic scattering structure functions at small x [30]. This involves very few parameters, and provides comprehensive description of deep inelastic scattering data at $x \leq 10^{-2}$. The description of F_2 in deep inelastic scattering is shown in Fig. 6. It should be noted that in the CGC description of deep inelastic scattering, the gluon distribution function is the Fock space distribution of gluons inside a hadron. It can never become negative. In the description of the F_2 data, the gluon distribution function is not becoming small at small Q^2 as is the case in some linear evolution fits. This is intuitively reasonable since we have no reason to expect that the Fock space distribution of gluons in a hadron should become small at small Q^2 .

The Color Glass Condensate description may also be applied to diffractive deep inelastic scattering, and with the same parameters that describe deep inelastic scattering does an excellent job of describing the data. In addition, there are measurements of the longitudinal structure function, a quantity directly proportional to the gluon density. Conventional descriptions that use linear DGLAP evolution equations are somewhat challenged by this data, but the CGC description naturally fits the data.

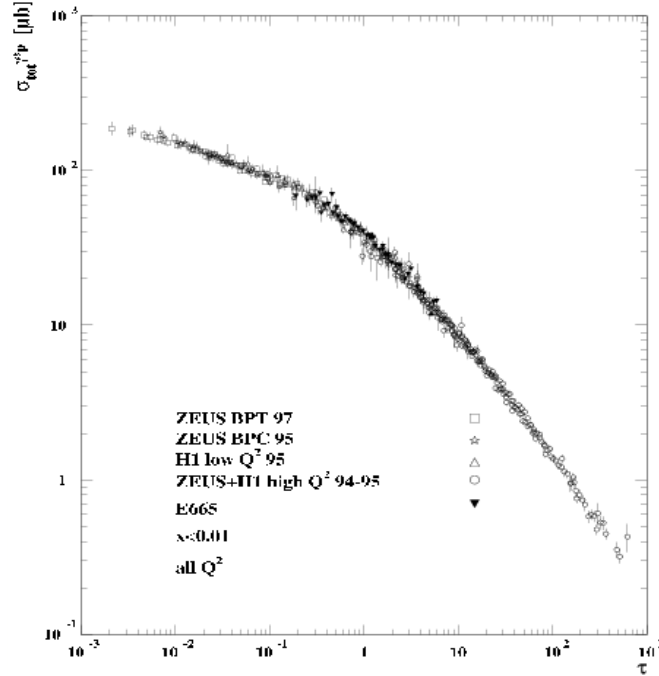


Fig. 5. The geometric scaling in deep inelastic scattering.

To summarize, the CGC description of deep inelastic scattering at small x naturally describes F_2 , F_L and diffractive data. It is a successful phenomenology. Why is the CGC therefore not accepted as the standard description? The problem is that the linear evolution DGLAP descriptions describe F_2 adequately, except in the region where the perturbative computations most probably breaks down. They do not do a very good job on the low Q^2 F_L data, but this is where there is a fair uncertainty in the data. The diffractive data is naturally described in the CGC framework, but there are other successful models. Ultimately, there is no consensus within the deep inelastic scattering community that the CGC is needed in order to describe the data.

2.2. The CGC and Heavy Ion Collisions

2.2.1. Multiplicities in RHIC Nuclear Collisions

One of the early successes of the CGC was the description of multiplicity distributions in deep inelastic scattering[31]–[33]. Recall that the phase

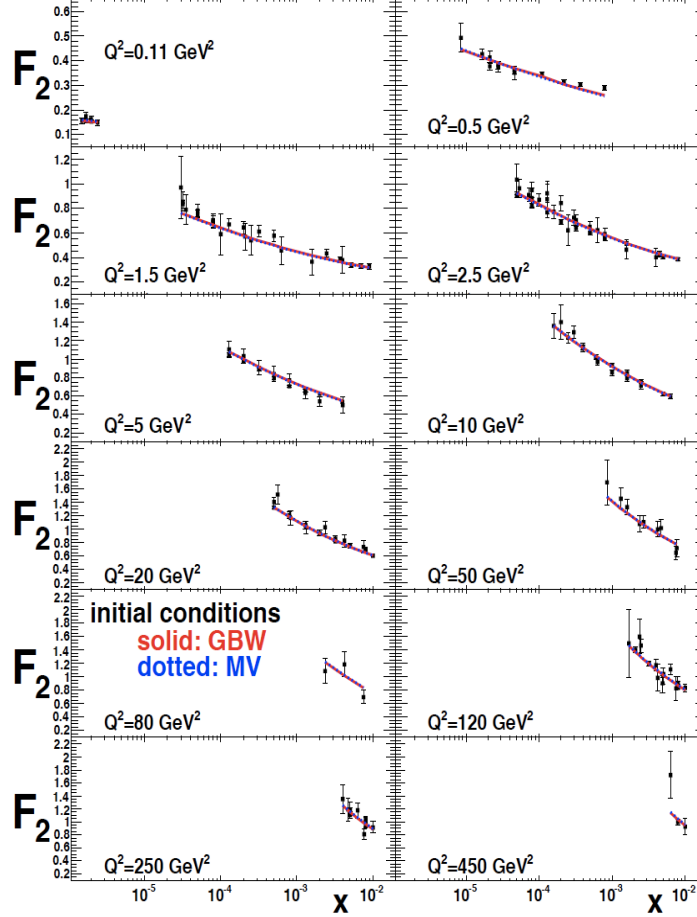


Fig. 6. The CGC description of F_2 data in deep inelastic scattering.

space distribution of gluons up to the saturation momentum is of order $Q_{sat}^2/\alpha_S(Q_{sat})$. We will assume that the distribution of initially produced gluons is proportional to this distribution of gluons in the hadron wavefunctions of the colliding nuclei and further, that the multiplicity of produced gluon is proportional to the final state distribution of pions. We get

$$\frac{1}{\sigma} \frac{dN}{dy} \sim \frac{1}{\alpha_S(Q_{sat})} Q_{sat}^2 \sim A^{1/3} x^{-\delta} \quad (3)$$

Here σ is the area of overlap of the two nuclei in the collision and A the number of nucleons that participate in the collision. $\sigma Q_{sat}^2 \sim A$ at low energies assumes no shadowing of nucleon parton distributions and is consistent with information concerning deep inelastic scattering on nuclear targets. In the collisions of nuclei one can directly measure the number of nucleonic participants in the collisions, a number that varies with the centrality of the collision. One can then compare the central region multiplicity with the number of participants so determined. Such a comparison is shown in [34]-[35] Fig. 7. The saturation description of Kharzeev and Nardi provides a good description of the centrality dependence of the collisions [31]. It also does well with the energy dependence. Refinements of this description can provide a good description of the rapidity distribution of produced particles [33].

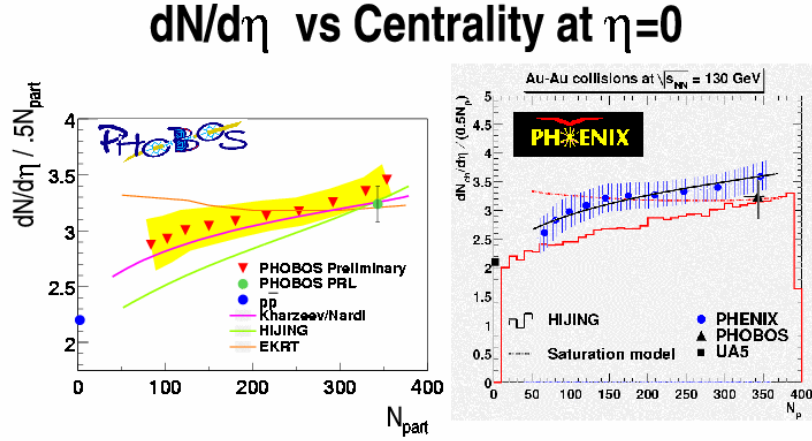


Fig. 7. The multiplicity as a function of the number of nucleon participants in heavy ion collisions.

2.2.2. Limiting Fragmentation

A general feature of high energy hadronic scattering is limiting fragmentation. If one measures the distribution of particles as a function of rapidity up to some fixed rapidity from the rapidity of one of the colliding particles, then the distribution is independent of collision energy. The region over which this scaling occurs increases as the energy of the colliding particles increases. Such scaling is shown in Fig. 8. Such limiting fragmentation

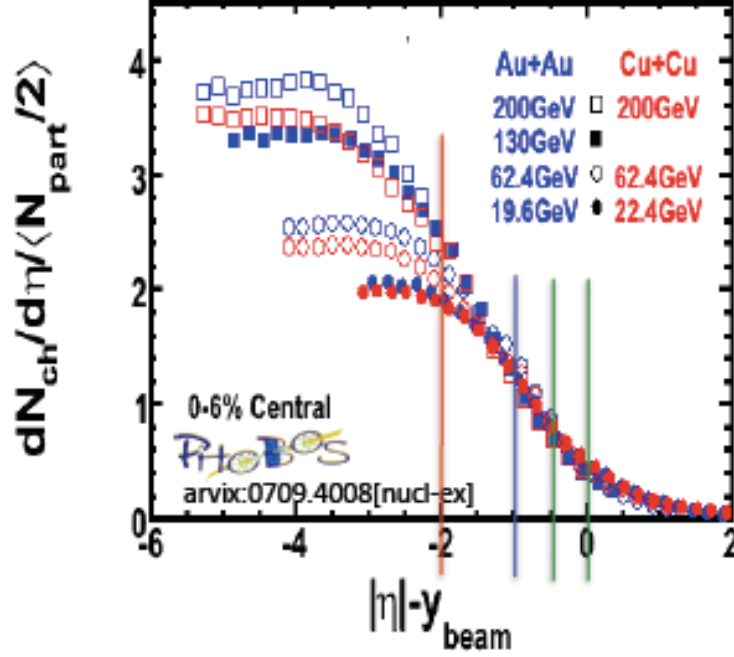


Fig. 8. Limiting fragmentation in RHIC nuclear collisions.

is natural in the CGC approach. For example in Fig. 8, we see that the region of limiting fragmentation increases as beam energy increases[35]. If we think of the region where there is limiting fragmentation as sources for fields at small more central rapidities, then we see that going to higher energies corresponds to treating a larger region as sources. In a renormalization group language, this simply means that one is integrating out fluctuations at less central rapidities, to generate an effective theory for the particles at more central rapidity. A quantitative description of limiting fragmentation within the theory of the CGC is found in Ref. [36].

2.2.3. Single Particle Distributions in dAu Collisions

Some of the early predictions of the CGC were generic features of the single particle inclusive distributions seen in hadron-nucleus collisions. There are two competing effects. The first is multiple scattering of a hadron as it traverses a nucleus. This effect is included in the CGC gluon distributions as an enhancement of the gluon distribution for p_T at transverse momentum

of the order of the saturation momentum, with a corresponding depletion at smaller momentum. There is little effect at high p_T . The other effect is that in the evolution of the gluon distribution to small x , the saturation momentum acts as a cutoff in the bremsstrahlung like integrals that generate such small x gluons. Nuclei have a larger saturation momentum than do hadrons, so the small x gluon distribution for nuclei will be suppressed relative to that for hadrons. Put another way, this effect will generate a suppression for more central collisions. The sum of these effects is shown in Fig. 9[37]-[42]. The different curves correspond to different rapidities of the produced particle, beginning with the top curve being near the fragmentation region of the nucleus. As one evolve further in rapidity, the enhancement at intermediate transverse momentum disappears and is replaced by a smooth curve with an overall suppression of produced particles.

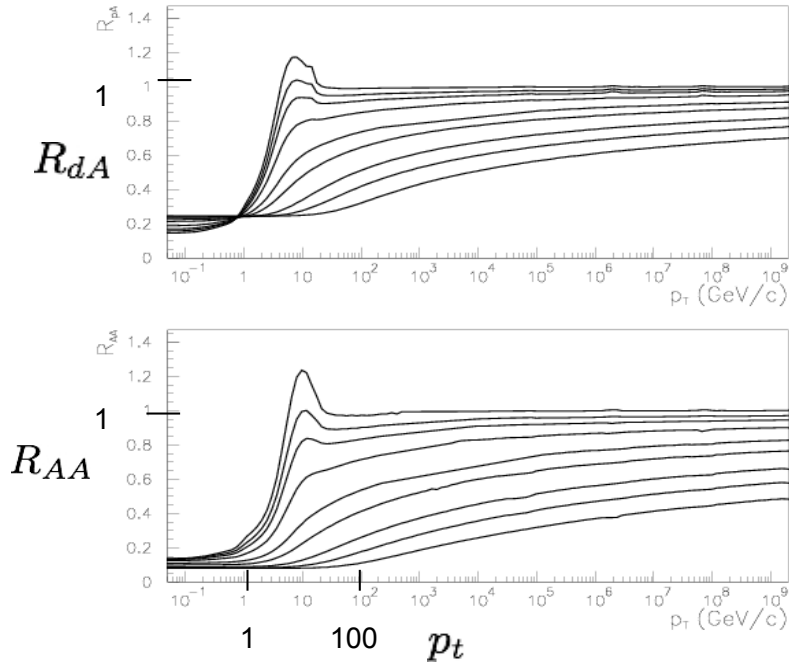


Fig. 9. The ratio of particles emitted in dA and AA collisions to that in proton due to CGC effects.

The pattern of suppression suggested by the Color Glass Condensate was first seen in dAu collisions in the Brahms collaboration[43], and later confirmed by the other experiments [34],[35],[44]. The Brahms experiments

demonstrated that in the nuclear target fragmentation region that at intermediate p_T there was an enhancement in R_{dA} as a function of centrality, but in the deuteron fragmentation region, there was a depletion as a function of centrality. The CGC provided the only model that predicted such an effect, and it remains the only theory that can quantitatively explain the suppression seen in the deuteron fragmentation region.

2.2.4. Heavy Quark and $J\Psi$ Production

If the saturation momentum is small compared to a quark mass, it can be treated as very heavy. It should have perturbative incoherent production cross sections. If the saturation momentum is large compared to a quark mass, the quarks should be thought of as light mass. Cross sections for production should be coherent, and for example in pA collisions, scale as $A^{2/3}$. In the deuteron fragmentation region of dAu collisions we would expect suppression of heavy quark and charmonium cross sections relative to the nuclear fragmentation region. In Fig. 10, the ratio of central to peripheral cross sections for J/Ψ production is shown as a function of centrality and rapidity. Note the strong suppression in the forward region for central collisions, as expected from the CGC. Precise computations are difficult for the charm quark since its mass is close to the saturation momentum. Such computations are in agreement with the data at forward rapidity[45]-[47].

2.2.5. Two Particle Correlations

The Glasma flux tubes induced by the collision of two hadrons will generate long range correlations in rapidity. In heavy ion collisions, this may be seen in forward backward correlations, as measured in STAR. The correlation increases in strength with higher energy collisions or more central collisions. This is expected in the CGC-Glasma description because for more central collisions the saturation momentum is bigger, so that the system is more correlated. (The coupling becoming weaker means the system is more classical, and therefore the leading order contribution associated with Glasma flux tubes becomes relatively more important.) Such forward-backward correlations are shown in Fig. 11 as a function of rapidity and centrality[48]-[49]. The value of the correlation coefficient b can be shown to be bounded $b \leq 1/2$.

Such two particle correlations in the Glasma can generate ridge like structures seen in two particle correlation experiments in azimuthal angle and rapidity[50]-[51]. The long range rapidity correlation is intrinsic to the Glasma. The angular correlation might be generated by flow effects at later times in the collision, by opacity and trigger bias effects, or by intrinsic angular correlations associated with the decay of Glasma flux tubes[52]-[56].

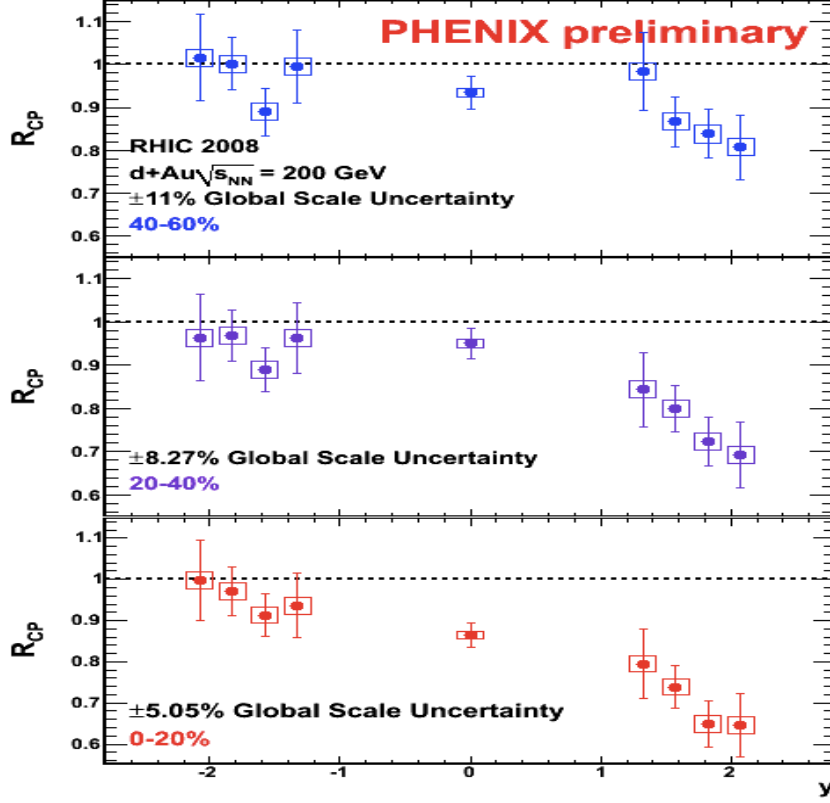


Fig. 10. The J/Ψ production cross section as a function of centrality and rapidity.

2.2.6. The Negative Binomial Distribution

The decay of a single Glasma flux tube generates a negative binomial distribution of produced particles[57]. A sum of negative binomial distributions is again a negative binomial distribution. Such a form of the distribution describes the RHIC data well. It is difficult with the heavy ion data to isolate those effects due to an intrinsic negative binomial distribution and those due to impact parameter. It is possible to isolate the effects of impact parameter, but it demands a high statistics study.

2.2.7. Two Particle Azimuthal Angular Correlations in dA Collisions

The CGC will de-correlate forward-backward angular correlations when the the transverse momentum of produced particles is of order the saturation momentum[58]-[60]. This is because near the produced particles get

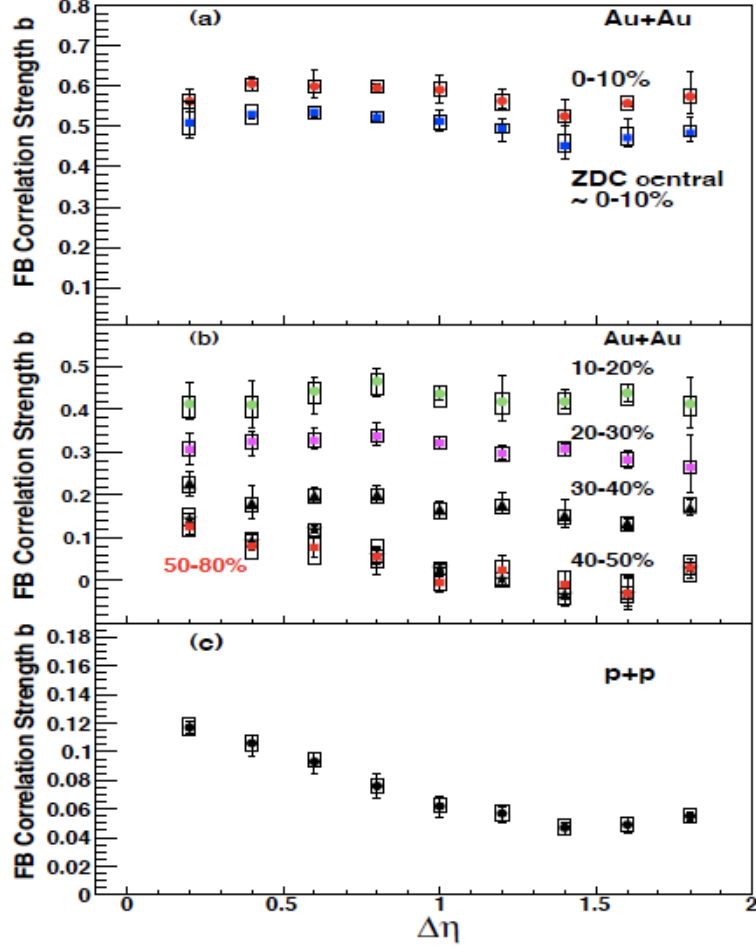


Fig. 11. The strength of forward backward correlations as a function of rapidity and centrality.

momentum from the CGC and therefore are not back-to-back correlated. In dAu collisions such an effect will be largest at forward rapidities near the fragmentation region of the deuteron, since this corresponds to the smallest values of x for the nuclear target. This kinematic region is least affected by multiple scattering on the nucleus. This effect has been seen by the STAR and PHENIX collaborations[61]-[62]. There is a good quantitative description by Tuchun and by Albacete and Marquet,[59]-[60] as shown in the figure 12

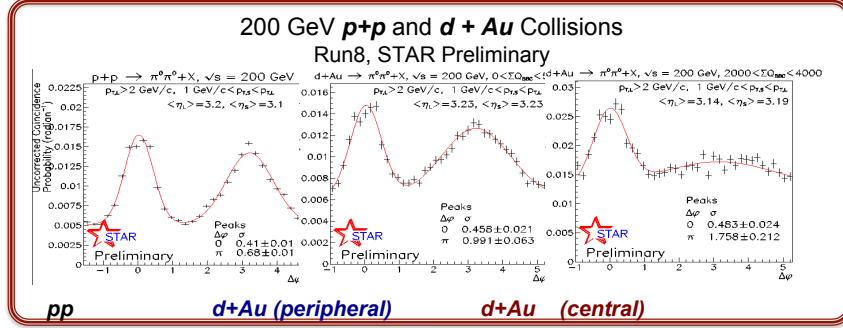


Fig. 12. Forward rapidity, forward backward angular correlations in dAu collisions as a function of centrality.

2.3. Concluding Comments on the CGC and the Glasma

There is now a wide variety of experimental data largely consistent with the CGC and Glasma based description. There is a well developed theoretical framework that provides a robust phenomenology of both electro-hadron scattering and hadron scattering, There are new areas that are developing that I have not had time to discuss. One is the possibility to see effects of topological charge change in heavy ion collisions, the Chiral Magnetic Effect[63]. Another area is pp collisions at the LHC, where some work concerning recent experimental data was developed at this school[64].

3. Lecture II: Matter at High Temperature: The Quark Gluon Plasma

4. Matter at Finite Temperature

4.1. Introduction

In this lecture I will describe the properties of matter at high temperature. The discussion here will be theoretical. There is a wide literature on the phenomenology of the Quark Gluon Plasma and its possible description of heavy ion collisions at RHIC energies. The interested reader is referred to that literature. I will here develop the ideas of deconfinement, chiral symmetry restoration based in part on a simple description using the large number of colors limit of QCD.

4.2. Confinement

The partition function is

$$Z = \text{Tr } e^{-\beta H + \beta \mu_B N_B} \quad (4)$$

where the temperature is $T = 1/\beta$ and N_B is the baryon number and μ_B is the baryon number chemical potential. Operator expectation values are

$$\langle O \rangle = \frac{\text{Tr } O e^{-\beta H + \beta \mu_B N_B}}{Z} \quad (5)$$

Under the substitution $e^{-\beta H} \rightarrow e^{-itH}$, the partition function becomes the time evolution operator of QCD. Therefore, if we change $t \rightarrow it$, and redefine zeroth components of fields by appropriate factors of i , and introduce Euclidean gamma matrices with anti-commutation relations

$$\{\gamma^\mu, \gamma^\nu\} = -2\delta^{\mu\nu} \quad (6)$$

then for QCD, the partition function has the path integral representation

$$Z = \int [dA][d\bar{\psi}][d\psi] \exp \left\{ - \int_0^\beta d^4x \left(\frac{1}{4} F^2 + \bar{\psi} \left[\frac{1}{i} \gamma \cdot D + m + i\mu_Q \gamma^0 \psi \right] \right) \right\} \quad (7)$$

Here the fermion field is a quark field so that the baryon number chemical potential is

$$\mu_Q = \frac{1}{N_c} \mu_B \quad (8)$$

This path integral is in Euclidean space and is computable using Monte Carlo methods when the quark chemical potential vanishes. If the quark chemical potential is non-zero, various contributions appear with different sign, and the Monte Carlo integrations are poorly convergent. Boundary conditions on the fields must be specified on account of the finite length of the integration in time. They are periodic for Bosons and anti-periodic for Fermions, and follow from the trace in the definition of the partition function.

A straightforward way to probe the confining properties of the QCD matter is to introduce a heavy test quark. If the free energy of the heavy test quark is infinite, then there is confinement, and if it is finite there is deconfinement. We shall see below that the free energy of an quark added to the system is

$$e^{-\beta F_q} = \langle L \rangle \quad (9)$$

where

$$L(\vec{x}) = \frac{1}{N_c} \text{Tr } P e^{i \int dt A^0(\vec{x}, t)} \quad (10)$$

So confinement means $\langle L \rangle = 0$ and deconfinement means that $\langle L \rangle$ is finite. The path ordered phase integration which defines the line operator L is shown in Fig. 20. Such a path ordered phase is called a Polyakov loop or Wilson line.



Fig. 13. The contour in the t plane which defines the Polyakov loop. The space is closed in time because of the periodic boundary conditions imposed by the definition of the partition function.

It is possible to prove that the free energy of a heavy static quark added to the system is given by Eqn. 9 using the effective action for a very heavy quark:

$$S_{HQ} = \int dt \bar{\psi}(\vec{x}, t) \frac{1}{i} \gamma^0 D^0 \psi(\vec{x}, t). \quad (11)$$

The Yang-Mills action is invariant under gauge transformations that are periodic up to an element of the center of the gauge group. The center of the gauge group is a set of diagonal matrices matrix $Z_p = e^{2\pi i p/N} \bar{I}$ where \bar{I} is an identity matrix. The quark contribution to the action is not invariant, and $L \rightarrow Z_p L$ under this transformation. In a theory with only dynamical gluons, the energy of a system of n quarks minus antiquarks is invariant under the center symmetry transformation only if n is an integer multiple of N . Therefore, when the center symmetry is realized, the only states of finite free energy are baryons plus color singlet mesons.

The realization of the center symmetry, $L \rightarrow Z_p L$ is equivalent to confinement. This symmetry is like the global rotational symmetry of a spin system, and it may be either realized or broken. At large separations, the correlation of a line and its adjoint, corresponding to a quark-antiquark pair is

$$\lim_{r \rightarrow \infty} \langle L(r) L^\dagger(0) \rangle = C e^{-\kappa r} + \langle L(0) \rangle \langle L^\dagger(0) \rangle \quad (12)$$

since upon subtracting a mean field term, correlation functions should vanish exponentially. Since

$$e^{-\beta F_{q\bar{q}}(r)} = \langle L(r) L^\dagger(0) \rangle \quad (13)$$

we see that in the confined phase, where $\langle L \rangle = 0$, the potential is linear, but in the unconfined phase, where $\langle L \rangle$ is non-zero, the potential goes to a constant at large separations.

The analogy with a spin system is useful. For the spin system corresponding to QCD without dynamical quarks, the partition function can be written as

$$Z = \int [dA] e^{-\frac{1}{g^2} S[A]} \quad (14)$$

The effective temperature of the spin system associated with the gluon fields is $T_{eff} \sim g^2$. By asymptotic freedom of the strong interactions, as real temperature gets larger, the effective temperature gets smaller. So at large real temperature (small effective temperature) we expect an ordered system, where the Z_N symmetry is broken, and there is deconfinement. For small real temperature corresponding to large effective temperature, there is disorder or confinement.

The presence of dynamical fermions breaks the Z_N symmetry. This is analogous to placing a spin system in an external magnetic field. There is no longer any symmetry associated with confinement, and the phase transition can disappear. This is what is believed to happen in QCD for physical masses of quarks. What was a first order phase transition for the theory in the absence of quarks becomes a continuous change in the properties of the matter for the theory with quarks.

Another way to think about the confinement-deconfinement transition is a change in the number of degrees of freedom. At low temperatures, there are light meson degrees of freedom. Since these are confined, the number of degrees of freedom is of order one in the number of colors. In the unconfined world, there are $2(N_c^2 - 1)$ gluons, and $4N_c N_f$ fermions where N_f is the number of light mass fermion families. The energy density scaled by T^4 is a dimensionless number and directly proportional to the number of degrees of freedom. We expect it to have the property shown in Fig. 14 for pure QCD in the absence of quarks. The discontinuity at the deconfinement temperature, T_d is the latent heat of the phase transition.

The energy density can be computed using lattice Monte Carlo methods. The result of such computation is shown in Fig. 15. The discontinuity present for the theory with no quarks becomes a rapid cross over when dynamical quarks are present.

The large N_c limit gives some insight into the properties of high temperature matter [65]-[68]. As $N_c \rightarrow \infty$, the energy density itself is an order parameter for the deconfinement phase transition. Viewed from the hadronic world, there is an amount of energy density $\sim N_c^2$ which must be inserted to surpass the transition temperature. At infinite N_c this cannot happen, as this involves an infinite amount of energy. There is a Hagedorn limiting temperature, which for finite N_c would have been the deconfinement temperature.

The Hagedorn limiting temperature can be understood from the view-

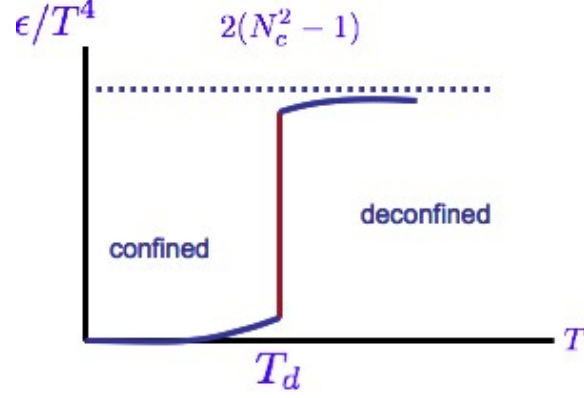


Fig. 14. The energy density scaled by T^4 for QCD in the absence of dynamical quarks.

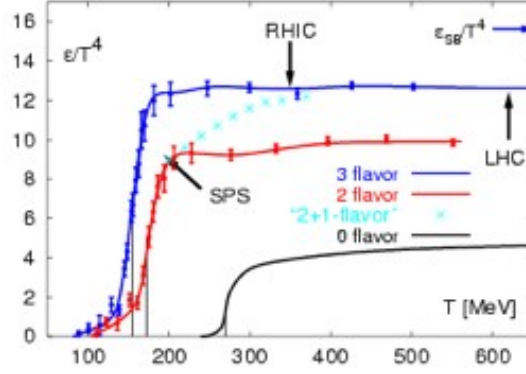


Fig. 15. The energy density scaled by T^4 measured in QCD from lattice Monte Carlo simulation. Here there are quarks with realistic masses.

point of the hadronic world as arising from an exponentially growing density of states. In a few paragraphs, we will argue that mesons and glueballs are very weakly interacting in the limit of large N_c . Therefore, the partition function is

$$Z = \int dm \rho(m) e^{-m/T} \quad (15)$$

Taking $\rho(m) \sim m^\alpha e^{\kappa m}$, so that

$$\langle m \rangle \sim \frac{1}{1/T - \kappa} \quad (16)$$

diverges when $T \rightarrow 1/\kappa$

4.3. A Brief Review of the Large N_c Limit

The large N_c limit for an interacting theory takes $N_c \rightarrow \infty$ with the 't Hooft coupling $g_{tHooft}^2 = g^2 N_c$ finite. This approximation has the advantage that the interactions among quarks and gluons simplify. For example, at finite temperature, the disappearance of confinement is associated with Debye screening by gluon loops, as shown in Fig. 16a. This diagram generates a screening mass of order $M_{screening}^2 \sim g_{tHooft}^2 T^2$. On the other hand the quark loop contribution is smaller by a power of N_c and vanishes in the large N_c limit.

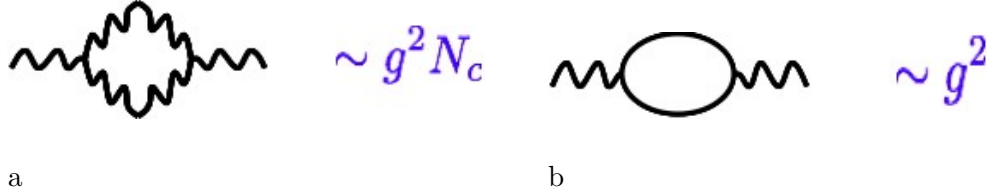


Fig. 16. a: The gluon loop contribution to the heavy quark potential. b: The quark loop contribution to the potential

To understand interactions, consider Fig. 17a. This corresponds to a mesonic current-current interaction through quarks. In powers of N_c , it is of order N_c . Gluon interactions will not change this overall factor. The three current interaction is also of order N_c as shown in Fig. 17b. The three meson vertex, G which remains after amputating the external lines, is therefore of order $1/\sqrt{N_c}$. A similar argument shows that the four meson interaction is of order $1/N_c$. Using the same arguments, one can show that the 3 glueball vertex is of order $1/N_c$ and the four glueball interaction of order $1/N_c^2$.

These arguments show that QCD at large N_c becomes a theory of non-interacting mesons and glueballs. There are an infinite number of such states because excitations can never decay. In fact, the spectrum of mesons seen in nature does look to a fair approximation like non-interacting particles. Widths of resonances are typically of order 200 MeV , for resonances with masses up to several GeV .

4.4. Mass Generation and Chiral Symmetry Breaking

QCD in the limit of zero quark masses has a $U(1) \times SU_L(2) \times SU_R(2)$ symmetry. (The $U_5(1)$ symmetry is explicitly broken due to the axial anomaly.)

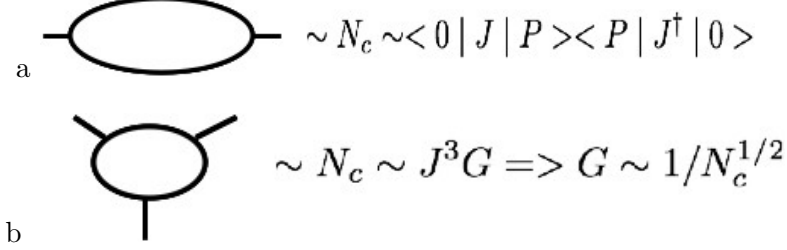


Fig. 17. a: The quark loop corresponding to a current-current interaction. b: A quark loop corresponding to a three current interaction.

Since the pion field, $\bar{\psi}\tau^a\gamma_5\psi$ is generated by an $SU_{L-R}(2)$ transformation of the sigma field, $\bar{\psi}\psi$, the energy (or potential) in the space of the pion-sigma field is degenerate under this transformation. In nature, pions have anomalously low masses. This is believed to be a consequence of chiral symmetry breaking, where the σ field acquires an expectation value, and the pion fields are Goldstone bosons associated with the degeneracy of the potential under the chiral rotations.

Such symmetry breaking can occur if the energy of a particle-antiparticle pair is less than zero, as shown in Fig. 18. On the left of this figure is the naive vacuum where the negative energy states associated with quarks are filled. The right hand side of the figure corresponds to a particle-hole excitation, corresponding to a sigma meson. Remember that a hole in the negative energy sea corresponds to an antiparticle with the opposite momentum and energy. If the σ meson excitation has negative energy, the system is unstable with respect to forming a condensate of these mesons.

At sufficiently high temperature, the chiral condensate might melt. Indeed this occurs [69]. For QCD, the chiral and deconfinement phase transition occur at the same temperature. At a temperature of about 170 – 200 MeV, both the linear potential disappears and chiral symmetry is restored. It is difficult to make a precise statement about the identification of the chiral and deconfinement phase transitions, since as argued above, for QCD with quarks, there is not a real phase transition associated with deconfinement [70]–[71]. Also, when quarks have finite masses, as they do in nature, chiral symmetry is not an exact symmetry, and there need be no strict phase transition associated with its restoration. Nevertheless, the cross over is quite rapid, and there are rapid changes in both the potential and the sigma condensate $\langle \bar{\psi}\psi \rangle$ at temperatures which are in a narrow range.

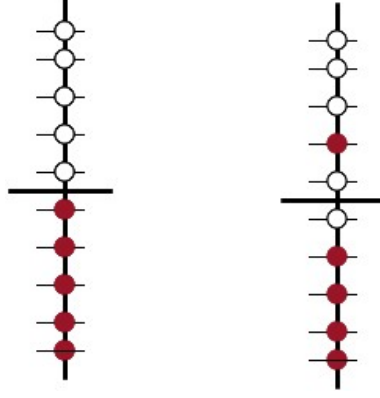


Fig. 18. The energy levels of the Dirac equation. Unfilled states are open circles and filled states are solid circles. For the free Dirac equation, negative energy states are filled and positive energy states are unoccupied, as shown on the left hand side. A mesonic excitation corresponding to a particle hole pair is shown on the right hand side.

5. Lecture III: Matter at High Baryon Number Density: Quarkyonic Matter

I now turn to a discussion of the phase diagram of QCD at finite baryon number density.

In the large N_c limit of QCD, the nucleon mass is of order N_c [65]-[67]. This means that in the confined phase of hadronic matter, for baryon chemical potential $\mu_B \leq M_N$, the baryon number density is essentially zero:

$$\langle N_B \rangle \sim e^{(\mu_B - M_N)/T} \sim e^{-N_c} \quad (17)$$

For temperatures above the de-confinement phase transition the baryon number is non-zero since there the baryon number density is controlled by $e^{-M_q/T} \sim 1$, and quark masses are independent of N_c . For sufficiently large chemical potential the baryon number density can be nonzero also. The Hadronic Matter phase of QCD is characterized in large N_c by zero baryon number density, but at higher density there is a new phase.

In the large N_c limit, fermion loops are suppressed by a factor of $1/N_c$. Therefore the contribution to Debye screening from quarks cannot affect the quark potential until

$$M_{Debye}^2 \sim \alpha_{t'Hooft} \mu_{quark}^2 / N_c \sim \Lambda_{QCD}^2 \quad (18)$$

Here the quark chemical potential is $\mu_B = N_c \mu_{quark}$. The relationship involving the Debye mass means there is a region parametrically large chemi-

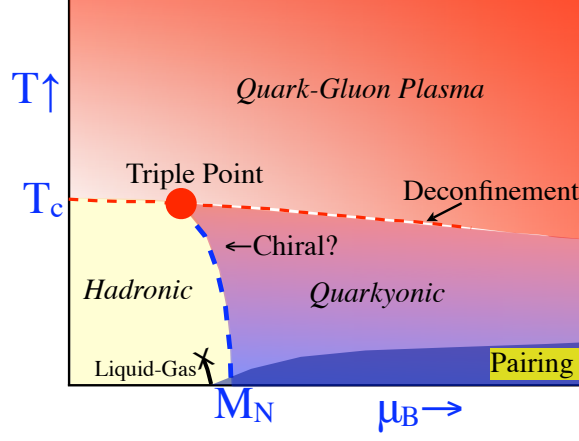


Fig. 19. The revised phase diagram of QCD

cal potential $M_N \leq \mu_B \leq \sqrt{N_c} M_N$ where matter is confined, and has finite baryon number. This matter is different than either the Hadronic Matter or the De-Confined Phases. It is called Quarkyonic because it exists at densities parametrically large compared to the QCD scale, where quark degrees of freedom are important, but it is also confined so the degrees of freedom may be thought of also as those of confined baryons[73]-[74].

The width of the transition region between the Hadronic phase and the Quarkyonic phase is estimated by requiring that the baryon number density become of order $N_B/V \sim k_{Fermi}^3 \sim \Lambda_{QCD}^3$. Recall that the baryon chemical potential is $\mu_B \sim M_N + k_f^2/2M_N$ for small k_F , so that the width of the transition in μ_B is very narrow, of order $1/N_c$. This is $\delta\mu_{quark} \sim 1/N_c^2$ when expressed in terms of μ_{quark} which is the finite variable in the large N_c limit.

The transition from Hadronic Matter to that of the Quark Gluon Plasma may be thought of as a change in the number of degrees of freedom of matter. Hadronic Matter at low temperatures has 3 pion degrees of freedom. The quark gluon plasma has of order $2(N_c^2 - 1)$ degrees of freedom corresponding to gluons and $4N_c$ degrees of freedom for each light mass quark. The change in degrees of freedom is of order N_c^2 in the large N_c limit. At very high baryon number densities, the quarks in the Fermi sea interact at short distances, and although strictly speaking are confined, behave like free quarks. The number of degrees of freedom is therefore of order N_c . Each phase has different numbers of degrees of freedom, and is presumably separated from the other by a rapid crossover. Quarkyonic matter is confined

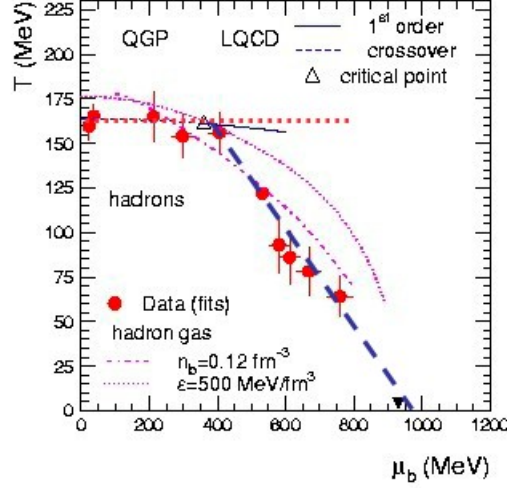


Fig. 20. Chemical potentials and temperatures at decoupling.

and therefore thermal excitations such as mesons, glueballs, and Fermi surface excitations must be thought of as confined. The quarks in the Fermi sea are effectively weakly interacting since their interactions take place at short distances. So in some sense, the matter is “de-confined” quarks in the Fermi sea with confined glueball, mesons and Fermi surface excitations[75].

In Hadronic Matter, chiral symmetry is broken and in Deconfined Matter it is broken. In Quarkyonic Matter chiral symmetry is broken by the formation of charge density waves from binding of quark and quark hole excitations near the Fermi surface[76]. In order that the quark hole have small relative momentum to the quark, the quark hole must have momentum opposite to that of the quark. This means the quark-quark hole excitation has total net momentum, and therefore the finite wavelength of the corresponding bound state leads to a breaking of translational invariance. The chiral condensate turns out to be a chiral spiral where the chiral condensate rotates between different Goldstone boson as one moves through the condensate[77]. Such condensation may lead to novel crystalline structures[78].

A figure of the hypothetical phase diagram of QCD is shown in Fig. 19 for $N_c = 3$. Also shown is the weak liquid-gas phase transition, and the phase associated with color superconductivity. Although the color superconducting phase cannot coexist with quarkyonic matter in infinite N_c , for finite N_c there is such possibility. The lines on this phase diagram might correspond to true phase transitions or rapid cross overs. The confinement-deconfinement transition is known to be a cross over. In the FPP-NJL

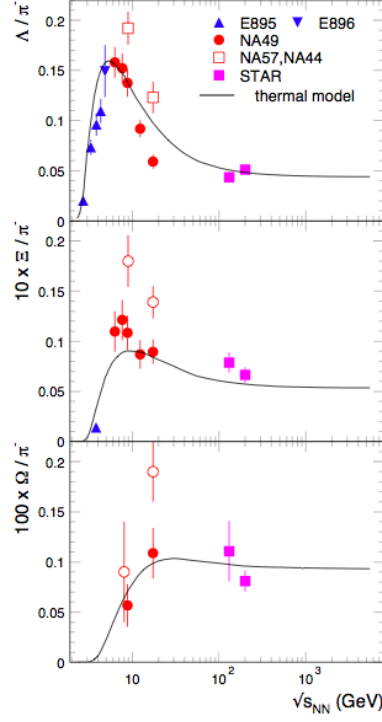


Fig. 21. Ratios of abundances of various particles .

model[79]-[81], the Hadronic-Quarkyonic transition is first order[82], but nothing is known from lattice computations. If as we conjecture, there is region where chiral symmetry is broken by translationally non-invariant modes, then this region must be surrounded by a line of phase transitions. I call this region Happy Island because it is an island of matter in the $\mu_B - T$ plane.

A remarkable feature of this plot is the triple point where the Hadronic Matter, Deconfined Matter and Quarkyonic Matter all meet[83]. This triple point is reminiscent of the triple point for the liquid, gas and vapor phases of water.

Since we expect a rapid change in the number of degrees of freedom across the transitions between these forms of matter, an expanding system crossing such a transition will undergo much dilution would undergo much dilution at a fixed value of temperature or baryon chemical potential[?]-[?]. One might expect in heavy ions to see decoupling of particle number changing processes at this transition, and the abundances of produced particles will be characteristic of the transition. In Fig. 20

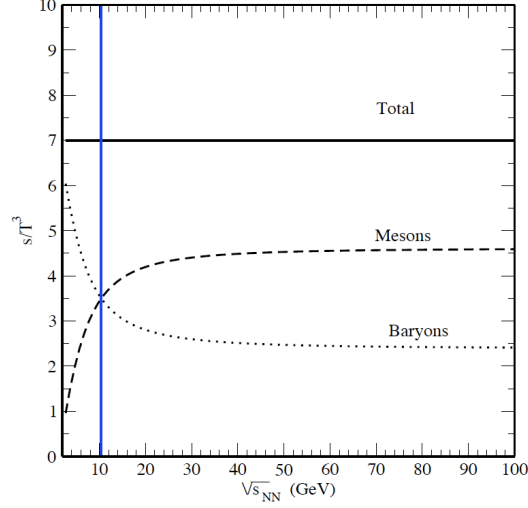


Fig. 22. Energy density stored in baryons compared to that stored in mesons.

In the Fig. 20, the expectations for the confinement-deconfinement transition are shown with the dotted red line. It is roughly constant with the baryon chemical potential, and the constant value of temperature is taken from lattice estimates. The dark dashed curve represents $\mu_B - T = \text{const} \times M_N$, corresponding to a simple model for the Quarkyonic transition. Such a very simple description does remarkably well.

A triple point is suggested at a baryon chemical potential near 400 MeV, and temperature near 160 MeV. This corresponds to a center of mass energy for Pb-Pb collisions of 9-10 GeV. This is near where there are anomalies in the abundances of ratios of particles[84], as shown in Fig. 21. Shown are fits using statistical models of abundances of particles using chemical potentials and temperature extracted from experimental data. The sharp peak reflects the change in behavior as one proceeds along the dashed line of Fig. 20 corresponding to the Quarkyonic transition and joins to the dotted red line of the deconfinement transition

It is remarkable that the value of beam energy where this occurs corresponds to the hypothetical triple point of Fig. 20, and that this is the density where the energy density stored in baryons becomes equal to that stored in mesons, Fig. 22,

Acknowledgments

I gratefully acknowledge the organizers of the 50'th Crakow School of Theoretical Physics, in particular, Michal Praszalowicz, for making this wonderful and extraordinary meeting. The research of L. McLerran is supported under DOE Contract No. DE-AC02-98CH10886.

REFERENCES

- [1] L. V. Gribov, E. M. Levin and M. G. Ryskin, Phys. Rept. **100**, 1 (1983).
- [2] A. H. Mueller and J. W. Qiu, Nucl. Phys. B **268**, 427 (1986).
- [3] L. D. McLerran and R. Venugopalan, Phys. Rev. D **49**, 2233 (1994) [arXiv:hep-ph/9309289].
- [4] L. D. McLerran and R. Venugopalan, Phys. Rev. D **49**, 3352 (1994) [arXiv:hep-ph/9311205].
- [5] E. Iancu and R. Venugopalan, arXiv:hep-ph/0303204.
- [6] A. Kovner, L. D. McLerran and H. Weigert, Phys. Rev. D **52**, 6231 (1995) [arXiv:hep-ph/9502289].
- [7] A. Kovner, L. D. McLerran and H. Weigert, Phys. Rev. D **52**, 3809 (1995) [arXiv:hep-ph/9505320].
- [8] A. Krasnitz and R. Venugopalan, Nucl. Phys. B **557**, 237 (1999) [arXiv:hep-ph/9809433].
- [9] A. Krasnitz and R. Venugopalan, Phys. Rev. Lett. **84**, 4309 (2000) [arXiv:hep-ph/9909203].
- [10] A. Krasnitz and R. Venugopalan, Phys. Rev. Lett. **86**, 1717 (2001) [arXiv:hep-ph/0007108].
- [11] A. Krasnitz, Y. Nara and R. Venugopalan, Phys. Rev. Lett. **87**, 192302
- [12] T. Lappi, Phys. Rev. C **67**, 054903 (2003) [arXiv:hep-ph/0303076].
- [13] T. Lappi and L. McLerran, Nucl. Phys. A **772**, 200 (2006) [arXiv:hep-ph/0602189].
- [14] J. D. Bjorken, Phys. Rev. D **27**, 140 (1983).
- [15] K. Dusling, T. Epelbaum, F. Gelis and R. Venugopalan, arXiv:1009.4363 [hep-ph].
- [16] A. M. Stasto, K. J. Golec-Biernat and J. Kwiecinski, Phys. Rev. Lett. **86**, 596 (2001) [arXiv:hep-ph/0007192].
- [17] I. Balitsky, Nucl. Phys. B **463**, 99 (1996) [arXiv:hep-ph/9509348].
- [18] J. Jalilian-Marian, A. Kovner, L. D. McLerran and H. Weigert, Phys. Rev. D **55**, 5414 (1997) [arXiv:hep-ph/9606337].
- [19] J. Jalilian-Marian, A. Kovner, A. Leonidov and H. Weigert, Nucl. Phys. B **504**, 415 (1997) [arXiv:hep-ph/9701284].

- [20] J. Jalilian-Marian, A. Kovner, A. Leonidov and H. Weigert, Phys. Rev. D **59**, 014014 (1999) [arXiv:hep-ph/9706377].
- [21] J. Jalilian-Marian, A. Kovner and H. Weigert, Phys. Rev. D **59**, 014015 (1999) [arXiv:hep-ph/9709432].
- [22] Y. V. Kovchegov, Phys. Rev. D **60**, 034008 (1999) [arXiv:hep-ph/9901281].
- [23] E. Iancu, A. Leonidov and L. D. McLerran, Nucl. Phys. A **692**, 583 (2001) [arXiv:hep-ph/0011241].
- [24] E. Iancu, A. Leonidov and L. D. McLerran, Phys. Lett. B **510**, 133 (2001) [arXiv:hep-ph/0102009].
- [25] E. Ferreira, E. Iancu, A. Leonidov and L. McLerran, Nucl. Phys. A **703**, 489 (2002) [arXiv:hep-ph/0109115].
- [26] A. H. Mueller and D. N. Triantafyllopoulos, Nucl. Phys. B **640**, 331 (2002) [arXiv:hep-ph/0205167].
- [27] E. Iancu, K. Itakura and L. McLerran, Nucl. Phys. A **708**, 327 (2002) [arXiv:hep-ph/0203137].
- [28] J. L. Albacete and Y. V. Kovchegov, Phys. Rev. D **75**, 125021 (2007) [arXiv:0704.0612 [hep-ph]].
- [29] I. Balitsky and G. A. Chirilli, Phys. Rev. D **77**, 014019 (2008) [arXiv:0710.4330 [hep-ph]].
- [30] J. L. Albacete, N. Armesto, J. G. Milhano and C. A. Salgado, Phys. Rev. D **80**, 034031 (2009) [arXiv:0902.1112 [hep-ph]].
- [31] D. Kharzeev and M. Nardi, Phys. Lett. B **507**, 121 (2001) [arXiv:nucl-th/0012025].
- [32] K. J. Eskola, K. Kajantie, P. V. Ruuskanen and K. Tuominen, Nucl. Phys. B **570**, 379 (2000) [arXiv:hep-ph/9909456].
- [33] D. Kharzeev, E. Levin and M. Nardi, Phys. Rev. C **71**, 054903 (2005) [arXiv:hep-ph/0111315].
- [34] K. Adcox *et al.* [PHENIX Collaboration], Nucl. Phys. A **757**, 184 (2005) [arXiv:nucl-ex/0410003].
- [35] B. B. Back *et al.*, Nucl. Phys. A **757**, 28 (2005) [arXiv:nucl-ex/0410022].
- [36] F. Gelis, A. M. Stasto and R. Venugopalan, Eur. Phys. J. C **48**, 489 (2006) [arXiv:hep-ph/0605087].
- [37] R. Baier, A. Kovner and U. A. Wiedemann, Phys. Rev. D **68**, 054009 (2003) [arXiv:hep-ph/0305265].
- [38] J. L. Albacete, N. Armesto, A. Kovner, C. A. Salgado and U. A. Wiedemann, Phys. Rev. Lett. **92**, 082001 (2004) [arXiv:hep-ph/0307179].
- [39] D. Kharzeev, Y. V. Kovchegov and K. Tuchin, Phys. Rev. D **68**, 094013 (2003) [arXiv:hep-ph/0307037].
- [40] D. Kharzeev, Y. V. Kovchegov and K. Tuchin, Phys. Lett. B **599**, 23 (2004) [arXiv:hep-ph/0405045].
- [41] J. Jalilian-Marian, Nucl. Phys. A **748**, 664 (2005) [arXiv:nucl-th/0402080].

- [42] E. Iancu, K. Itakura and D. N. Triantafyllopoulos, Nucl. Phys. A **742**, 182 (2004) [arXiv:hep-ph/0403103].
- [43] I. Arsene *et al.* [BRAHMS Collaboration], Nucl. Phys. A **757**, 1 (2005) [arXiv:nucl-ex/0410020].
- [44] J. Adams *et al.* [STAR Collaboration], Nucl. Phys. A **757**, 102 (2005) [arXiv:nucl-ex/0501009].
- [45] D. Kharzeev, E. Levin, M. Nardi and K. Tuchin, Phys. Rev. Lett. **102**, 152301 (2009) [arXiv:0808.2954 [hep-ph]].
- [46] D. Kharzeev, E. Levin, M. Nardi and K. Tuchin, Nucl. Phys. A **826**, 230 (2009) [arXiv:0809.2933 [hep-ph]].
- [47] B. Z. Kopeliovich, I. K. Potashnikova, H. J. Pirner and I. Schmidt, arXiv:1008.4272 [hep-ph].
- [48] B. I. Abelev *et al.* [STAR Collaboration], Phys. Rev. Lett. **103**, 172301 (2009) [arXiv:0905.0237 [nucl-ex]].
- [49] T. Lappi and L. McLerran, Nucl. Phys. A **832**, 330 (2010) [arXiv:0909.0428 [hep-ph]].
- [50] E. V. Shuryak, Phys. Rev. C **76**, 047901 (2007) [arXiv:0706.3531 [nucl-th]].
- [51] A. Dumitru, F. Gelis, L. McLerran and R. Venugopalan, Nucl. Phys. A **810**, 91 (2008) [arXiv:0804.3858 [hep-ph]].
- [52] S. Gavin, L. McLerran and G. Moschelli, Phys. Rev. C **79**, 051902 (2009) [arXiv:0806.4718 [nucl-th]].
- [53] R. P. G. Andrade, F. Grassi, Y. Hama and W. L. Qian, arXiv:1008.4612 [nucl-th].
- [54] K. Werner, I. Karpenko, T. Pierog, M. Bleicher and K. Mikhailov, arXiv:1004.0805 [nucl-th].
- [55] B. Alver and G. Roland, Phys. Rev. C **81**, 054905 (2010) [Erratum-ibid. C **82**, 039903 (2010)] [arXiv:1003.0194 [nucl-th]].
- [56] A. Dumitru, K. Dusling, F. Gelis, J. Jalilian-Marian, T. Lappi and R. Venugopalan, arXiv:1009.5295 [hep-ph].
- [57] F. Gelis, T. Lappi and L. McLerran, Nucl. Phys. A **828**, 149 (2009) [arXiv:0905.3234 [hep-ph]].
- [58] D. Kharzeev, E. Levin and L. McLerran, Nucl. Phys. A **748**, 627 (2005) [arXiv:hep-ph/0403271].
- [59] K. Tuchin, Nucl. Phys. A **846**, 83 (2010) [arXiv:0912.5479 [hep-ph]].
- [60] J. L. Albacete and C. Marquet, arXiv:1009.3215 [hep-ph].
- [61] E. Braidot and f. t. S. Collaboration, arXiv:1008.3989 [nucl-ex].
- [62] B. Meredith, Nucl. Phys. A **830**, 595C (2009) [arXiv:0907.4832 [nucl-ex]].
- [63] D. E. Kharzeev, L. D. McLerran and H. J. Warringa, Nucl. Phys. A **803**, 227 (2008) [arXiv:0711.0950 [hep-ph]].
- [64] L. McLerran and M. Praszalowicz, Acta Phys. Polon. B **41**, 1917 (2010) [arXiv:1006.4293 [hep-ph]].
- [65] G. 't Hooft, Nucl. Phys. B **72**, 461 (1974).

- [66] G. 't Hooft, Nucl. Phys. B **75**, 461 (1974).
- [67] E. Witten, Nucl. Phys. B **160**, 57 (1979).
- [68] C. B. Thorn, Phys. Lett. B **99**, 458 (1981).
- [69] F. Karsch, Lect. Notes Phys. **583**, 209 (2002) [arXiv:hep-lat/0106019].
- [70] A. Bazavov *et al.*, Phys. Rev. D **80**, 014504 (2009) [arXiv:0903.4379 [hep-lat]].
- [71] S. Borsanyi *et al.*, arXiv:1007.2580 [hep-lat].
- [72] M. G. Alford, Ann. Rev. Nucl. Part. Sci. **51**, 131 (2001) [arXiv:hep-ph/0102047].
- [73] L. McLerran and R. D. Pisarski, Nucl. Phys. A **796**, 83 (2007) [arXiv:0706.2191 [hep-ph]].
- [74] Y. Hidaka, L. D. McLerran and R. D. Pisarski, Nucl. Phys. A **808**, 117 (2008) [arXiv:0803.0279 [hep-ph]].
- [75] P. Castorina, R. V. Gavai and H. Satz, arXiv:1003.6078 [Unknown].
- [76] D. V. Deryagin, D. Y. Grigoriev and V. A. Rubakov, Int. J. Mod. Phys. A **7**, 659 (1992).
- [77] T. Kojo, Y. Hidaka, L. McLerran and R. D. Pisarski, arXiv:0912.3800 [Unknown].
- [78] T. Kojo, R. Pisarski and A. Tsvelik, private communication.
- [79] K. Fukushima, Phys. Lett. B **591**, 277 (2004) [arXiv:hep-ph/0310121].
- [80] N. Kaiser, S. Fritsch and W. Weise, Nucl. Phys. A **697**, 255 (2002) [arXiv:nucl-th/0105057].
- [81] R. D. Pisarski, Phys. Rev. D **62**, 111501 (2000) [arXiv:hep-ph/0006205].
- [82] L. McLerran, K. Redlich and C. Sasaki, Nucl. Phys. A **824**, 86 (2009) [arXiv:0812.3585 [hep-ph]].
- [83] A. Andronic *et al.*, arXiv:0911.4806 [Unknown].
- [84] M. Gazdzicki and M. I. Gorenstein, Acta Phys. Polon. B **30**, 2705 (1999) [arXiv:hep-ph/9803462].